

RESEARCH

Open Access



Quercetin-primed MSC exosomes synergistically attenuate osteoarthritis progression

Mingfeng Lu^{1,2†}, Aiju Lou^{3†}, Junqing Gao^{1,2}, Shilin Li^{1,2}, Lilei He^{1,2}, Weifeng Fan^{1,2*} and Lilian Zhao^{1,2*}

Abstract

Background Osteoarthritis (OA), a degenerative joint disease characterized by cartilage degradation and inflammation, lacks effective disease-modifying therapies. Quercetin, a bioactive flavonoid derived from Traditional Chinese Medicine, exhibits anti-inflammatory and chondroprotective properties but is limited by poor bioavailability. Mesenchymal stem cell-derived exosomes (MSC-Exos) offer a promising strategy for targeted drug delivery and cartilage regeneration.

Methods Bone marrow-derived MSC exosomes (Que-Exo) were isolated after preconditioning with quercetin (1 μ M, 24 h). Their effects were evaluated in IL-1 β -stimulated chondrocytes via RT-qPCR, Western blot, transcriptomics, and proteomics. An ACLT-induced OA mouse model received intra-articular injections of Que-Exo, with cartilage integrity assessed by Safranin O staining and OARSI scoring.

Results Que-Exo significantly reduced IL-1 β -induced pro-inflammatory markers (MMP9 and COX-2) and restored cartilage repair genes (SOX9 and Collagen II) compared to untreated exosomes. Multi-omics analyses revealed activation of PI3K-AKT signaling and glutathione metabolism pathways. In vivo, Que-Exo mitigated cartilage degradation and preserved proteoglycan content.

Conclusions Quercetin-preconditioned MSC exosomes synergistically enhance chondroprotection and anti-inflammatory effects, offering a novel therapeutic strategy for OA by combining herbal bioactive compounds with exosome-mediated delivery.

Keywords Osteoarthritis, Quercetin, Engineered exosomes, Chondroprotection, Multi-omics analysis

[†]Mingfeng Lu and Aiju Lou contributed equally to this work.

*Correspondence:

Weifeng Fan
13106664870@163.com
Lilian Zhao
zhaolilian@163.com

¹The Eighth Clinical Medical College of Guangzhou University of Chinese Medicine, Foshan, Guangdong 528000, China

²Foshan Hospital of Traditional Chinese Medicine, Foshan, Guangdong 528000, China

³Department of Rheumatology, Liwan Central Hospital of Guangzhou, Guangzhou, Guangdong 510030, China



Introduction

Osteoarthritis (OA), a multifaceted degenerative joint pathology, manifests as a complex interplay of cartilage matrix metalloproteinase-mediated extracellular matrix degradation, synovial macrophage-driven chronic inflammation, and aberrant mechanotransduction in subchondral bone [1, 2]. This triad of pathological processes creates a self-perpetuating cycle of joint destruction, affecting over 300 million patients globally [3, 4]. Despite advances in molecular diagnostics, current therapeutic paradigms remain trapped in a palliative model—NSAIDs mask pain while accelerating cartilage erosion through COX-2 mediated prostaglandin cascades, intra-articular corticosteroids transiently suppress inflammation but inhibit cartilage progenitor cell activation, and joint arthroplasty, though effective in end-stage disease, carries substantial risks of prosthesis failure and septic complications [5, 6]. The absence of disease-modifying OA drugs (DMOADs) capable of simultaneously interrupting inflammatory signaling cascades while activating cartilage anabolic pathways underscores a critical unmet clinical need.

Traditional Chinese Medicine (TCM) offers a poly-pharmacological approach particularly suited to OA's multidimensional pathogenesis [7]. Some studies reveal that TCM formulations like Du-Huo-Ji-Sheng-Tang exert chondroprotection through multi-level regulation of Rho/NF- κ B-mediated inflammations [8], Notch1/NLRP3 oxidative stress response [9], and SMAD 1/5/8-ERK signaling bone remodeling balance [10]. Among TCM-derived bioactive molecules, quercetin—a diphenolic flavonoid with a 3,3',4',5,7-pentahydroxyflavone structure—exhibits unique pleiotropic effects: (1) Competitive inhibition of TLR4/Myd88 complex formation [11–13]; (2) Activation of SIRT1-mediated deacetylation to enhance FOXO3-driven antioxidant gene expression [14]; (3) Modulation of Wnt/ β -catenin signaling to prevent hypertrophic chondrocyte differentiation [15]. However, quercetin's therapeutic potential is paradoxically constrained by poor solubility, low bioavailability, and rapid systemic clearance, limiting its therapeutic efficacy [16, 17].

Recent advances in regenerative medicine highlight the potential of mesenchymal stem cell-derived exosomes (MSC-Exos) as novel treatments for many diseases, such as periodontitis [18], ischemic heart disease [19], COVID-19 [20] and Alzheimer's disease [21]. Studies demonstrate that MSC-Exos contain bioactive components including growth factors (VEGF, PDGF-AA), and anti-inflammatory cytokines (IL-1RA), which collectively enhance tissue repair through promoting cell proliferation and stem cell migration [22]. The emergence of mesenchymal stem cell-derived exosomes (MSC-Exos)

as endogenous nanotherapeutics (40–100 nm diameter) presents a paradigm-shifting drug delivery strategy [23].

These nanosized extracellular vesicles exhibit inherent advantages, including immunomodulation, anti-inflammatory activity, and tissue repair capabilities, particularly in promoting cartilage regeneration [24, 25]. Notably, exosomes can serve as natural carriers for bioactive molecules, enhancing drug stability and targeted delivery [25]. These phospholipid bilayer vesicles naturally encapsulate therapeutic payloads including: (i) Cartilage-targeting miRNAs (miR-140-3p promoting HIF-1 α [26]; miR-125a-5p inhibiting E2F2 [27]); (ii) Tissue repair proteins (s-GAG [28]); (iii) Metabolic regulators (down-regulating METTL3 combating ferroptosis [29]).

Building on this, we hypothesize that quercetin preconditioning reprograms MSC-Exos to amplify anti-inflammatory and cartilage regenerative effects while overcoming quercetin's pharmacokinetic barriers. Preconditioning MSCs with quercetin could modulate exosomal cargo, to enhance their chondroprotective and anti-OA functions. This study aims to investigate the efficacy and mechanisms of quercetin-preconditioned MSC-Exos in OA treatment. We propose a dual strategy: (1) utilizing exosomes to improve quercetin's bioavailability and cartilage targeting, and (2) elucidating how quercetin reprograms exosomal contents to activate regenerative pathways. Through integrated transcriptomic and proteomic analyses, we will identify key molecular networks regulated by quercetin-exosomes interactions. Our approach bridges traditional herbal medicine with cutting-edge exosomes technology, offering a novel paradigm for OA therapy.

Materials and methods

Preparation and identification of engineering exosomes derived from quercetin-preconditioned BMSCs

Bone marrow-derived mesenchymal stem cells (BMSCs) were isolated from the femurs and tibias of 6-week-old C57BL/6 mice. The bone marrow was flushed out using phosphate-buffered saline (PBS) containing 1% penicillin-streptomycin. The collected marrow cells were cultured in complete α -MEM (alpha minimum essential medium) supplemented with 10% fetal bovine serum (FBS, Gibco, USA) and 1% penicillin-streptomycin. The cells were maintained at 37 °C in a humidified incubator with 5% CO₂. Quercetin (Sigma-Aldrich, USA) was dissolved in DMSO to prepare a stock solution. MSCs at passage 3 were treated with varying concentrations of quercetin (1 μ M [30]) for 24 h. The control group was treated with an equivalent volume of DMSO. After the preconditioning period, the culture medium was replaced with fresh growth medium, and the cells were incubated for another 48 h to allow for exosomes secretion. Exosomes were isolated from the culture

supernatants of quercetin-preconditioned MSCs using a commercial exosomes isolation kit (ExoQuick-TC, USA). Briefly, after removing the cell debris by centrifugation at $300 \times g$ for 10 min, the supernatant was further centrifuged at $2,000 \times g$ for 30 min to eliminate larger vesicles. The resulting supernatant was subjected to ultracentrifugation at $100,000 \times g$ for 90 min at 4°C to pellet the exosomes. The exosomes pellet was then resuspended in PBS and stored at -80°C until further characterization. The size distribution and zeta potential of the exosomes were analyzed using Dynamic Light Scattering (DLS) and Zeta potential measurement, respectively. Exosomes samples were diluted in PBS and analyzed using a Zetasizer Nano (Malvern Instruments, UK).

Transmission electron microscope (TEM)

To confirm the morphology of the isolated exosomes, a portion of the exosomes' suspension was negatively stained with 2% uranyl acetate and observed under a transmission electron microscope (Hitachi HT7700, Japan). Exosomes samples were placed on copper grids, air-dried, and then imaged at an acceleration voltage of 80 kV. Exosomes size, shape, and the presence of the typical cup-shaped morphology were assessed.

Culture and treatment of mouse chondrocytes

The isolation of primary mouse chondrocytes was performed using the trypsin-collagenase digestion method [31]. Cartilage tissues were harvested aseptically from the knee and hip joints of C57BL/6 mice (7 days old), minced into small pieces, and digested with 0.2% type II collagenase (Sigma, USA) at 37°C for 4–6 h, until complete digestion and the formation of a single-cell suspension. The digestion was terminated using DMEM/F12 medium supplemented with 10% fetal bovine serum (FBS) and 1% penicillin-streptomycin, followed by centrifugation at 1000 rpm for 5 min to collect the cells. The cell pellet was resuspended in DMEM/F12 complete medium and seeded into 6-well plates or culture flasks. The cells were maintained in an incubator at 37°C with 5% CO_2 , and the culture medium was replaced every 2–3 days. To establish an in vitro inflammatory stimulation model, primary chondrocytes at 70–80% confluence were pre-cultured in serum-free medium for 12 h, followed by treatment with 10 ng/mL recombinant mouse interleukin-1 β (IL-1 β , PeproTech, USA) together with 10 $\mu\text{g}/\text{mL}$ Exo or

Que-Exo for 24 h [32]. All subsequent in vitro analyses were performed after this standardized 24-hour treatment period to ensure consistency. The control group was treated with serum-free medium only.

RT-qPCR

Total RNA was extracted from cells using RNAiso Plus reagent (TAKARA, Japan). RNA concentration and purity were determined using a NanoDrop spectrophotometer. Reverse transcription was performed using the PrimeScript™ RT Reagent Kit (TAKARA, Japan), where 1 μg of RNA was converted into cDNA. Real-time PCR was conducted using the TB Green™ Premix Ex Taq™ II (TAKARA, Japan) with specific primers for the target genes. The reaction was run in a Bio-Rad CFX96 thermal cycler, with an initial denaturation at 95°C for 30 s, followed by 40 cycles of 95°C for 5 s and 60°C for 30 s. Gene expression was normalized to GAPDH and calculated using the $2^{-\Delta\Delta\text{Ct}}$ method. Data were obtained in triplicates and repeated at least three times. Each sample was analyzed in triplicate, and the experiments were repeated at least three times. The primer sequences used are shown in Table 1.

Western blot

Total proteins were extracted from cells using RIPA buffer (TAKARA, Japan) supplemented with protease inhibitors. After lysis and centrifugation ($12,000 \times g$, 15 min, 4°C), protein concentration was measured using the BCA Protein Assay Kit (Thermo Scientific, USA). Protein samples were mixed with SDS loading buffer, boiled, and separated by SDS-PAGE (10% gel). Proteins were transferred to PVDF membranes at 260 V for 2 h. Membranes were blocked with 5% non-fat milk in TBST for 1 h, then incubated with primary antibodies (overnight, 4°C). After washing, membranes were incubated with HRP-conjugated secondary antibodies for 1 h. Protein bands were detected using ECL substrate (Millipore, USA) and visualized using a chemiluminescence imaging system (Bio-Rad, USA). Band intensities were quantified using ImageJ software. The antibodies used are shown in Table 2.

Immunofluorescence staining

Immunofluorescence (IF) staining was performed to assess the expression of MMP9 and Collagen II (COL II) in chondrocytes. Cells were cultured on confocal dishes and treated with IL-1 β , Exo and Que-Exo. After the designated treatments, cells were washed with PBS and fixed with 4% paraformaldehyde at room temperature for 15 min. Cells were then permeabilized with 0.1% Triton X-100 for 10 min and blocked with 5% bovine serum albumin (BSA) for 1 h to prevent non-specific binding. Primary antibodies against MMP9, and COL II were

Table 1 The primer sequences

Gene	Forward primers (5'-3')	Reverse primers (5'-3')
<i>Col2a1</i>	GCAGAGATGGAGAACCTGGTA	AGCCTTCTCGTCATACCCCT
<i>Sox9</i>	GAGCCGGATCTGAAGAGGGA	GCTTGACGTGTGGCTTGTTTC
<i>Cox2</i>	GCCAGCAAAGCCTAGAGCAA	GCCTTCTGCAAGTCCAGGTTTC
<i>Mmp9</i>	CTGGACAGCCAGACACTAAAG	CTCGCGGCAAGTCTTCAGAG
<i>Gapdh</i>	CAGGAGCGAGACCCCACTAA	ATCACGCCACAGCTTCCAG

Table 2 The antibodies

	Brand	Catalog Number
Collagen II	Proteintech	28459-1-AP
SOX9	Abcam	ab185966
COX2	Proteintech	27308-1-AP
MMP9	Proteintech	10375-2-AP
GAPDH	Proteintech	60004-1-Ig
iNOS	Abcam	ab15323
TNF- α	Abcam	ab183218
MMP13	Abcam	ab315267
MMP3	Proteintech	17873-1-AP
HRP-conjugated Goat Anti-Rabbit IgG(H+L)	Proteintech	SA00001-2
HRP-conjugated Goat Anti-Mouse IgG(H+L)	Proteintech	SA00001-1
Goat Anti-Rabbit IgG H&L (Alexa Fluor® 488)	Abcam	ab150077
Goat Anti-Rabbit IgG H&L (Alexa Fluor® 594)	Abcam	ab150080

diluted in 1% BSA and incubated overnight at 4 °C. The next day, cells were washed with PBS and incubated with fluorescently labeled secondary antibodies (Alexa Fluor 488 or 594-conjugated) at room temperature for 1 h in the dark. Actin was stained with Actin-Tracker (Phalloidin, Green 488 or Red-594, Beyotime, China) at room temperature for 30 min in the dark. Nuclei were counterstained with DAPI (4',6-diamidino-2-phenylindole) for 5 min in the dark. Images were captured using a Confocal microscope (ZEISS LSM980, German) under identical settings for all groups. The antibodies used are shown in Table 2.

RNA-seq analysis

Total RNA was extracted from the treated cells using TRIzol Reagent (Invitrogen, USA) according to the manufacturer's protocol. After RNA extraction, the quality and concentration of the RNA were assessed using a NanoDrop spectrophotometer and RNA integrity was evaluated using an Agilent 2100 Bioanalyzer (Agilent Technologies, USA). Only RNA samples with an RNA Integrity Number (RIN) > 7 were used for sequencing. Subsequently, RNA samples were used for library construction and sequencing (LC-Bio Technology CO., Ltd., China). The libraries were constructed using the TruSeq Stranded mRNA Library Prep Kit (Illumina, USA) according to the manufacturer's instructions. Briefly, poly(A) mRNA was isolated from total RNA using magnetic oligo(dT) beads, followed by fragmentation, reverse transcription to cDNA, and adapter ligation. The cDNA libraries were then amplified and quality-checked before sequencing. Sequencing was performed on the Illumina NovaSeq 6000 platform, generating paired-end reads (150 bp). The raw sequencing data were processed and

analyzed for gene expression profiling and differential expression analysis.

Quantitative proteomics analysis

Total proteins were extracted using RIPA buffer (TAKARA, Japan) and quantified by the BCA Protein Assay Kit (Thermo Scientific, USA). Equal amounts of protein (50 μ g) were digested using the FASP method: reduction with DTT, alkylation with iodoacetamide, and overnight trypsin digestion (Promega, USA). Peptides were desalted using C18 spin columns (Thermo Scientific, USA), then reconstituted in 0.1% formic acid. The samples were analyzed by Orbitrap Astral High-Resolution Mass Spectrometry (Thermo Fisher Scientific, USA) coupled with an Easy-nLC 1200 system (Thermo Fisher Scientific, USA). The peptides were separated on a C18 column with a 120-minute gradient, and mass spectra were acquired in positive ion mode with a resolution of 120,000. Raw data were processed with MaxQuant software for protein identification and quantification. Differentially expressed proteins were analyzed using Perseus software, with statistical significance determined by t-test and ANOVA ($p < 0.05$).

Establishment and disposal of OA mouse model

8-week-old male C57BL/6 mice, purchased from the Guangdong Provincial Laboratory Animal Center, were housed under standard conditions with a 12-hour light/dark cycle and free access to food and water. Osteoarthritis (OA) was induced by anterior cruciate ligament transection (ACLT) under anesthesia with isoflurane. The mice were randomly divided into four groups ($n = 5$ per group): the Sham Surgery group, the ACLT + PBS injection group, the ACLT + Exo group, and the ACLT + Que-Exo group. In the ACLT groups, the anterior cruciate ligament was transected in the right knee. Mice received intra-articular injections of 2 μ g Exo or Que-Exo (resuspended in 5 μ L normal saline) twice weekly for 8 weeks, as previously validated for exosome efficacy in OA models. Sham and ACLT groups received 5 μ L normal saline alone under the same regimen.

H&E staining

After 8 weeks of treatment, knee joint tissues were collected and fixed in 4% paraformaldehyde (PFA) overnight at 4 °C. The fixed tissues were then decalcified in 10% ethylenediaminetetraacetic acid (EDTA) solution for 2 weeks, followed by dehydration in graded alcohol solutions. The tissues were embedded in paraffin and sectioned into 5- μ m-thick slices using a microtome.

For Hematoxylin and Eosin (H&E) staining, the paraffin sections were deparaffinized in xylene and rehydrated through a graded alcohol series. The sections were stained with hematoxylin for 5 min, followed by rinsing

in water and differentiation in 1% hydrochloric acid in ethanol. After staining with eosin for 2 min, the slides were dehydrated through alcohol, cleared in xylene, and mounted with a coverslip. Histological changes in the joint tissues were observed under a light microscope.

Safranin O/fast green staining

For Safranin O/Fast Green staining, the sections were deparaffinized and rehydrated as described above. The slides were stained with Safranin O solution for 10 min, followed by Fast Green solution for 5 min to counterstain the tissues. After washing in distilled water, the slides were dehydrated, cleared, and mounted with a coverslip. This staining was used to assess cartilage integrity and proteoglycan content in the knee joints. Following staining, the degree of OA severity was evaluated using the Osteoarthritis Research Society International (OARSI) scoring system, which assesses cartilage degeneration, subchondral bone changes, and synovial inflammation. Cartilage lesions were scored based on the extent of surface irregularity, loss of cartilage, and subchondral bone involvement, with a higher score indicating more severe OA changes. Scoring was conducted by two blinded researchers to ensure accuracy and consistency.

Statistical analysis

Data are presented as the mean \pm standard deviation (SD). Statistical analysis was performed using GraphPad Prism 8.0 (GraphPad Software, USA). Differences between two groups were analyzed using unpaired Student's t-test, while comparisons among multiple groups were performed using one-way analysis of variance (ANOVA) followed by Tukey's post hoc test for pairwise comparisons. A p-value of less than 0.05 ($p < 0.05$) was considered statistically significant. All experiments were repeated at least three times to ensure reproducibility.

Results

Characterization and evaluation of engineered exosomes derived from quercetin-preconditioned MSCs

In this study, we first used mass spectrometry to analyze the composition and content of Traditional Chinese Medicine Gu Bao Wan, and the results from Fig. 1A showed that quercetin was the most abundant component in Gu Bao Wan. Quercetin was then used to pre-treat BMSCs for 24 h, after which exosomes were extracted from the quercetin-pretreated BMSCs. The calibration curve for quercetin (Fig. 1B) demonstrated reliable quantification, and the mass spectrometry peak corresponding to quercetin (Fig. 1C) showed a clear signal with a high signal-to-noise ratio, confirming the successful detection of quercetin. The schematic diagram in Fig. 1D illustrates the process of quercetin pre-treatment of BMSCs and the subsequent exosomes extraction. Figure 1E presents

the TEM image of the extracted quercetin-pretreated BMSCs exosomes (Que-Exo), showing typical spherical morphology with a size of approximately 100 nm. The particle size distribution (Fig. 1F) and zeta potential measurements (Fig. 1G) confirmed that Que-Exo had a stable size and negative charge, ensuring good stability. Finally, Fig. 1H shows Western blot analysis for exosomes markers CD81 and CD63, confirming the successful isolation and quality of the exosomes.

Engineered exosomes improve inflammatory changes in chondrocytes caused by IL-1 β

In this experiment, the effects of quercetin-pretreated exosomes (Que-Exo) on gene and protein expression related to osteogenesis and inflammation were evaluated in IL-1 β -stimulated BMSCs. As shown in Fig. 2A, RT-qPCR analysis revealed that IL-1 β treatment significantly increased the expression of Mmp9, Cox-2, Sox9 and Collagen II mRNA compared to the control group. However, treatment with exosomes (Exo) and quercetin-pretreated exosomes (Que-Exo) significantly reduced the expression of Mmp9 and Cox-2, with the Que-Exo group showing the most substantial decrease. The expression of Sox9 and Collagen II mRNA, was also significantly upregulated in the Que-Exo group compared to both IL-1 β groups.

Similarly, western blot analysis (Fig. 2B and C) demonstrated that treatment with Exo and Que-Exo reduced the expression of MMP9 and COX-2, with Que-Exo exhibiting the strongest inhibitory effect. Additionally, SOX9 and Collagen II expression was significantly higher in the Que-Exo group compared to IL-1 β groups.

Immunofluorescence analysis (Fig. 2D) corroborated the protein expression profiles. Compared to the control group, IL-1 β -treated chondrocytes exhibited pronounced upregulation of MMP9 expression accompanied by significant downregulation of COL II. Exo-treated cells demonstrated partial mitigation of these pathological changes, with moderate reduction in MMP9 signal intensity and restoration of COL II expression. Notably, Que-Exo exhibited enhanced therapeutic efficacy, achieving near-baseline MMP9 levels and complete recovery of COL II deposition.

To further validate the hypothesis that Quercetin-preconditioned MSC-derived exosomes (Que-Exo) synergistically enhance chondroprotection and exert anti-inflammatory effects, we performed Western blot analysis to assess the expression of inflammatory markers (iNOS, TNF- α) and catabolic enzymes (MMP-3, MMP-13) in IL-1 β -stimulated chondrocytes. As shown in Figure S1, IL-1 β stimulation significantly upregulated the expression of iNOS, TNF- α , MMP-3, and MMP-13 compared with the control group. Treatment with Exo partially attenuated this upregulation, whereas Que-Exo

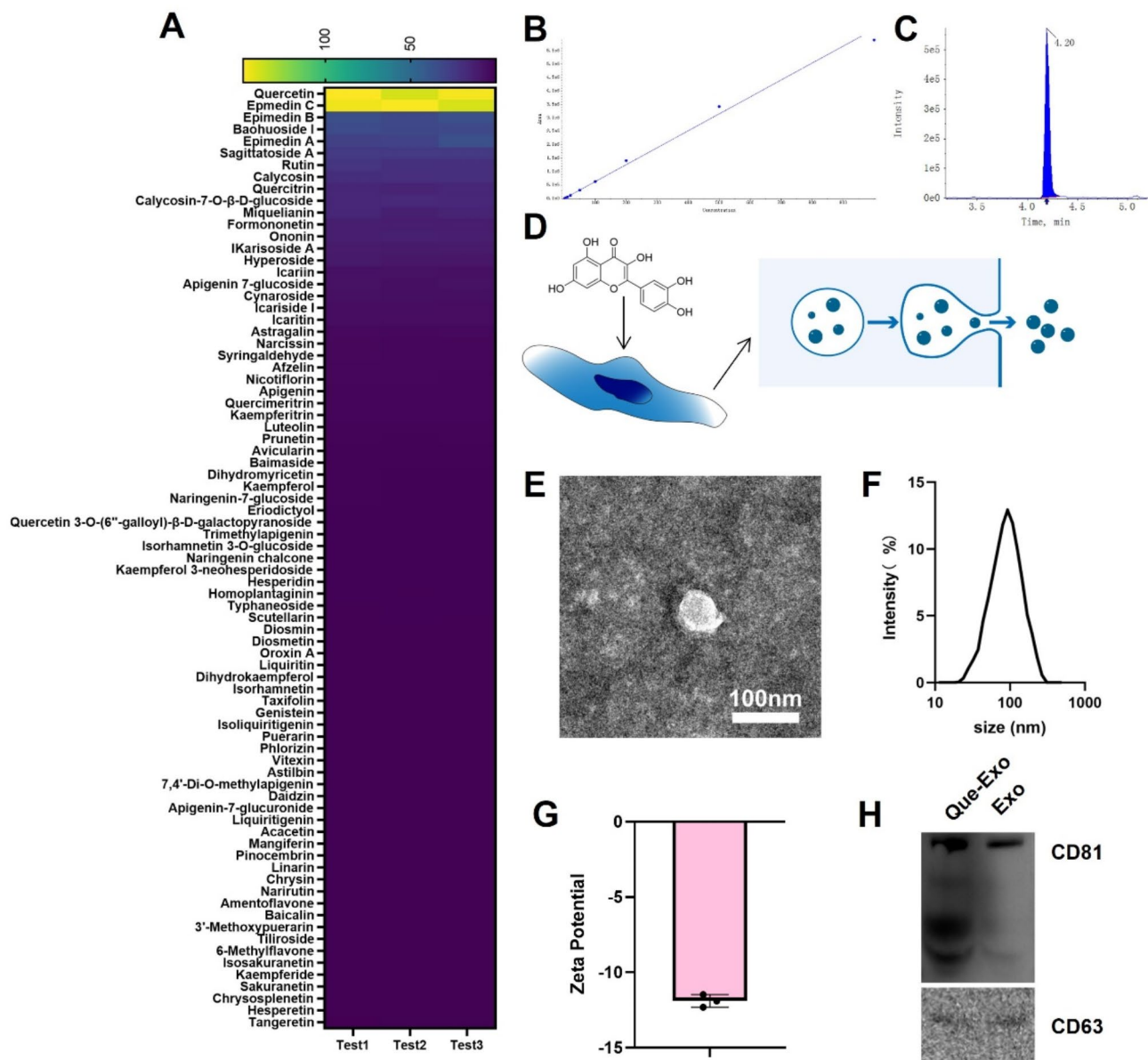


Fig. 1 Analysis of Gu Bao Wan and the characterization of Que-Exo. **(A)** Mass spectrometry results showing the composition and content of compounds in Gu Bao Wan. **(B)** Calibration curve for quercetin used for quantification. **(C)** Mass spectrometry peak for quercetin. **(D)** Schematic diagram illustrating the process of quercetin pre-treatment of BMSCs for 24 h followed by exosomes extraction. **(E)** TEM image of the Que-Exo. **(F)** Particle size distribution of Que-Exo. **(G)** Zeta potential of Que-Exo. **(H)** Western blot analysis of exosomes markers CD81 and CD63. The data are presented as mean \pm SD

treatment exhibited a significantly stronger suppressive effect on all tested markers. Notably, the expression levels of iNOS and TNF- α were markedly reduced in the Que-Exo group compared to the Exo group, indicating enhanced anti-inflammatory activity.

These findings support that Que-Exo possess superior therapeutic potential over unmodified exosomes in suppressing IL-1 β -induced inflammatory and catabolic responses, thereby contributing to enhanced chondroprotection.

Differential gene expression and pathway enrichment analysis in Que-Exo-treated chondrocytes

RNA sequencing was performed to systematically characterize the transcriptomic reprogramming effects of Que-Exo on IL-1 β -stimulated chondrocytes. Differential gene expression analysis revealed a significant change between the Que-Exo and Exo groups, with 752 upregulated and 89 downregulated genes (Fig. 3B). The Pearson correlation heatmap (Fig. 3A) confirmed a high correlation within the replicate groups, indicating consistency in the sample treatments. The volcano plot (Fig. 3C) further illustrated the distribution of upregulated (red) and

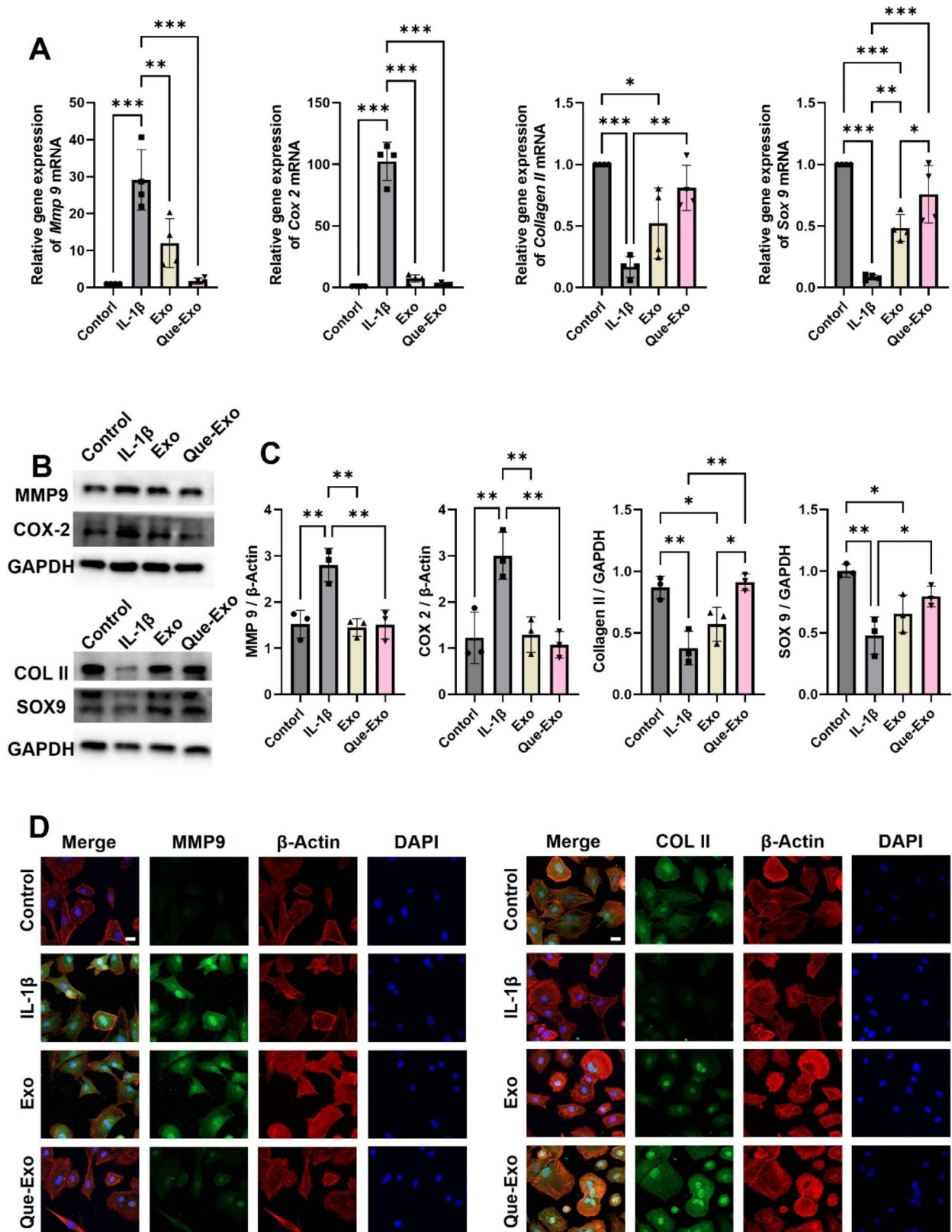


Fig. 2 Effect of quercetin-pretreated exosomes (Que-Exo) on gene and protein expression in IL-1 β -stimulated chondrocytes. **(A)** RT-qPCR analysis of the relative gene expression of Mmp9, Cox-2, Collagen II, and Sox9. **(B)** Western blot analysis of protein expression of MMP9, COX-2, Collagen II, and SOX9. **(C)** Quantification of protein expression from Western blot analysis. **(D)** Immunofluorescence staining for MMP9 and COL II; bar = 20 μ m. The data are presented as mean \pm SD. Statistical significance: * p < 0.05, ** p < 0.01, *** p < 0.001

(See figure on previous page.)

Fig. 4 Quantitative Proteomics Analysis of Que-Exo in IL-1 β -Stimulated Chondrocytes. **(A)** Subcellular localization analysis of differentially expressed proteins. **(B)** Bar plot illustrating the number of upregulated (472) and downregulated (474) proteins between the Que-Exo and IL-1 β groups. **(C)** Heatmap of differentially expressed proteins between Que-Exo and IL-1 β groups. **(D)** Volcano plot showing the differential expression of proteins between Que-Exo and IL-1 β groups. **(E)** InterPro enrichment analysis. **(F)** Gene Ontology (GO) enrichment analysis of differentially expressed proteins. **(G)** KEGG pathway enrichment analysis

downregulated (blue) genes, highlighting the substantial changes induced by Que-Exo treatment. Figure 3D displays a hierarchical clustering heatmap of differentially expressed genes between Que-Exo and IL-1 β groups.

KEGG pathway enrichment analysis (Fig. 3E) identified several pathways significantly affected by Que-Exo treatment, including cellular processes such as cell cycle regulation and neurotrophin signaling, as well as metabolic pathways such as drug metabolism and glutamate metabolism. Notably, the PI3K-AKT signaling pathway, a crucial regulator of cell survival, proliferation, and metabolism, was enriched. These findings suggest that Que-Exo treatment may influence a variety of biological processes, including cell proliferation, signaling, and metabolism. Furthermore, Gene Ontology (GO) enrichment analysis (Fig. 3F) categorized the enriched genes into biological processes, cellular components, and molecular functions, with biological processes related to RNA metabolic processes and cellular responses to stress being particularly prominent.

Differential protein expression and pathway enrichment analysis in Que-Exo-treated chondrocytes

Quantitative proteomics analysis identified 472 upregulated and 474 downregulated proteins between the Que-Exo and IL-1 β groups (Fig. 4B). The volcano plot (Fig. 4D) shows the distribution of differentially expressed proteins, with upregulated proteins in red and downregulated proteins in blue. Subcellular localization analysis (Fig. 4A) revealed that the majority of proteins were localized in the cytoplasm, followed by the membrane and nucleus. Heatmap analysis (Fig. 4C) showed distinct clustering of proteins between the Que-Exo and IL-1 β groups, indicating clear differences in protein expression profiles. InterPro enrichment analysis (Fig. 4E) identified enriched protein families and domains related to protein kinases and enzymes, highlighting their roles in signal transduction and metabolic processes. KEGG pathway enrichment analysis (Fig. 4G) revealed significant enrichment of the PI3K-AKT signaling pathway, along with pathways involved in cell cycle regulation and metabolism, suggesting key biological processes influenced by Que-Exo treatment. Gene Ontology (GO) enrichment analysis (Fig. 4F) categorized the differentially expressed proteins into biological processes such as cellular response to stress and RNA processing, cellular components like cytoplasm and nucleus, and molecular

functions including ATP binding and protein kinase activity.

Integrated transcriptomic and proteomic analysis of Que-Exo treatment in IL-1 β -Stimulated chondrocytes

Integrated analysis of transcriptomic and proteomic data revealed key insights into the molecular changes induced by Que-Exo in IL-1 β -stimulated chondrocytes. The scatter plot (Fig. 5A) shows the correlation between the log₂ fold change of differentially expressed genes and proteins, with genes and proteins that exhibit similar expression patterns being closely positioned. The Spearman correlation coefficient (Fig. 5B) further confirms the moderate correlation (median = 0.14) between gene expression and protein levels, suggesting some divergence between mRNA and protein regulation.

KEGG pathway enrichment analysis (Fig. 5C) highlighted several significantly enriched pathways, including glutathione metabolism, cytokine-cytokine receptor interaction, and drug metabolism by cytochrome P450, among others. These pathways are involved in critical processes such as oxidative stress response, immune signaling, and drug metabolism, indicating the wide-ranging effects of Que-Exo treatment on cellular function.

Gene Ontology (GO) enrichment analysis (Fig. 5D) further categorized the biological processes, cellular components, and molecular functions associated with the differentially expressed genes and proteins. Significant enrichment was observed in the extracellular region, membrane, and plasma membrane for cellular components, suggesting a major impact of Que-Exo on cellular structures involved in signaling and communication. Molecular functions related to calcium ion binding, collagen binding, and signaling receptor activity were also highly enriched, indicating potential roles in cellular signaling and extracellular matrix regulation (Fig. 5).

Differential GO and KEGG enrichment analysis in gene and protein expression across Que-Exo-treated chondrocytes

Further integrated analysis of transcriptomic and proteomic data revealed distinct biological insights into the effects of Que-Exo on IL-1 β -stimulated chondrocytes. In the group with downregulated genes and upregulated proteins (Fig. 6A-B), Gene Ontology (GO) enrichment analysis highlighted significant biological processes such as cellular response to stress, protein folding, and immune response. Enriched KEGG pathways included phagosome and cytokine-cytokine receptor interaction.

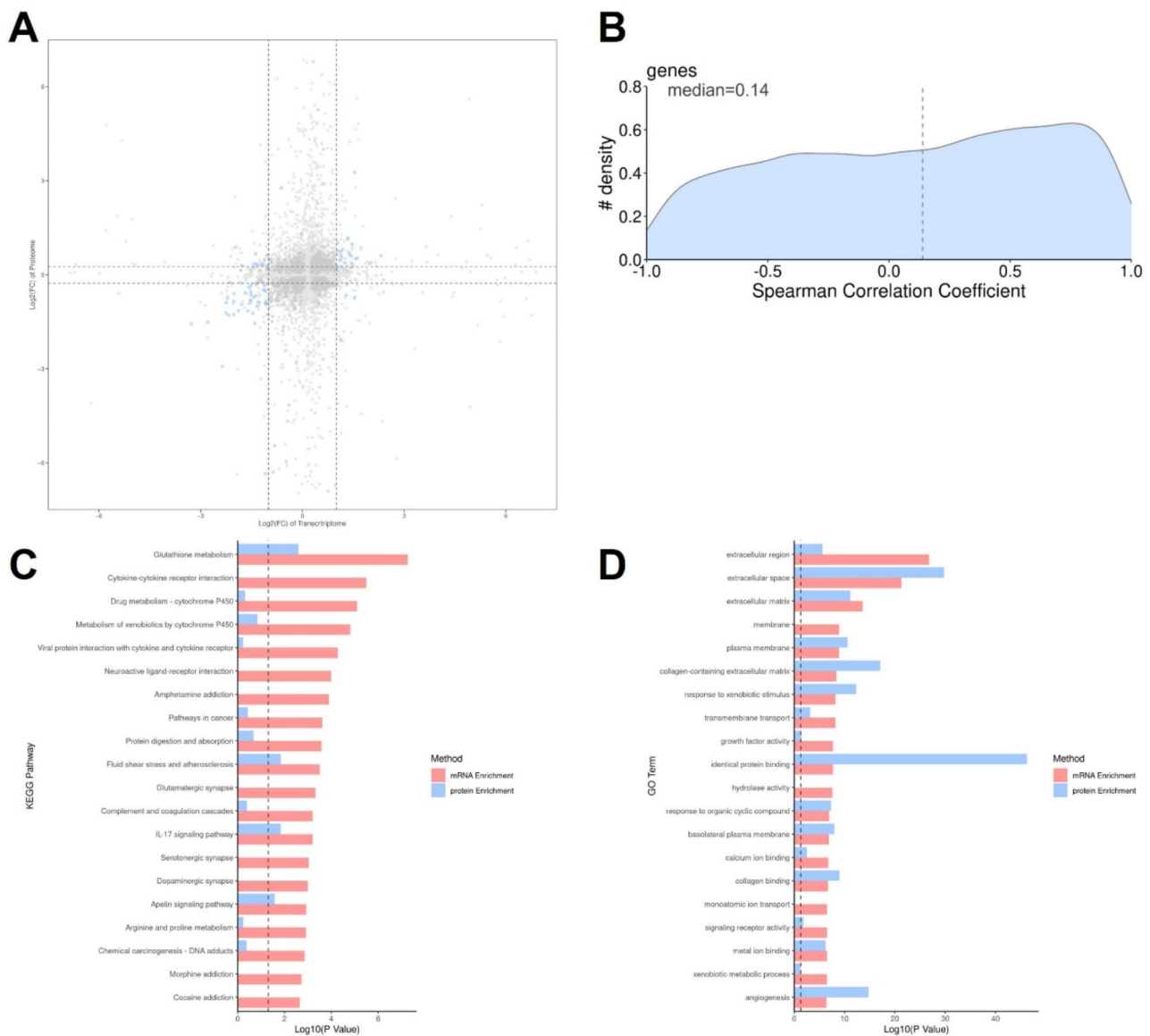


Fig. 5 Integrated Transcriptomic and Proteomic Analysis of Que-Exo in IL-1 β -Stimulated Chondrocytes. **(A)** Volcano plot. **(B)** Spearman correlation density plot. **(C)** KEGG pathway enrichment analysis comparing the transcriptomic and proteomic data. **(D)** GO enrichment analysis comparing the transcriptomic and proteomic data

For the upregulated genes and downregulated proteins group (Fig. 6C-D), GO enrichment analysis identified pathways such as response to oxidative stress and transmembrane transport, suggesting a cellular adaptation to stress and regulation of signaling. In the corresponding KEGG pathway analysis, EGFR signaling and MAPK signaling were significantly enriched, supporting the involvement of Que-Exo in cell signaling pathways.

In the downregulated genes and downregulated proteins group (Fig. 6E-F), GO enrichment analysis revealed enrichment in cell cycle regulation and cellular response to DNA damage, highlighting a potential effect of Que-Exo on cell cycle progression and DNA repair. KEGG

pathway analysis further identified proteasome pathways and glutathione metabolism, reflecting an influence on protein degradation and oxidative stress management.

Finally, for the upregulated genes and upregulated proteins group (Fig. 6G-H), GO enrichment analysis highlighted calcium ion binding and collagen binding, suggesting that Que-Exo treatment may impact signaling and extracellular matrix remodeling. KEGG pathway enrichment revealed significant pathways such as phagocytosis, PI3K-AKT signaling, and neuroactive ligand-receptor interaction, which are crucial for cellular survival, immune regulation, and tissue remodeling (Fig. 6).

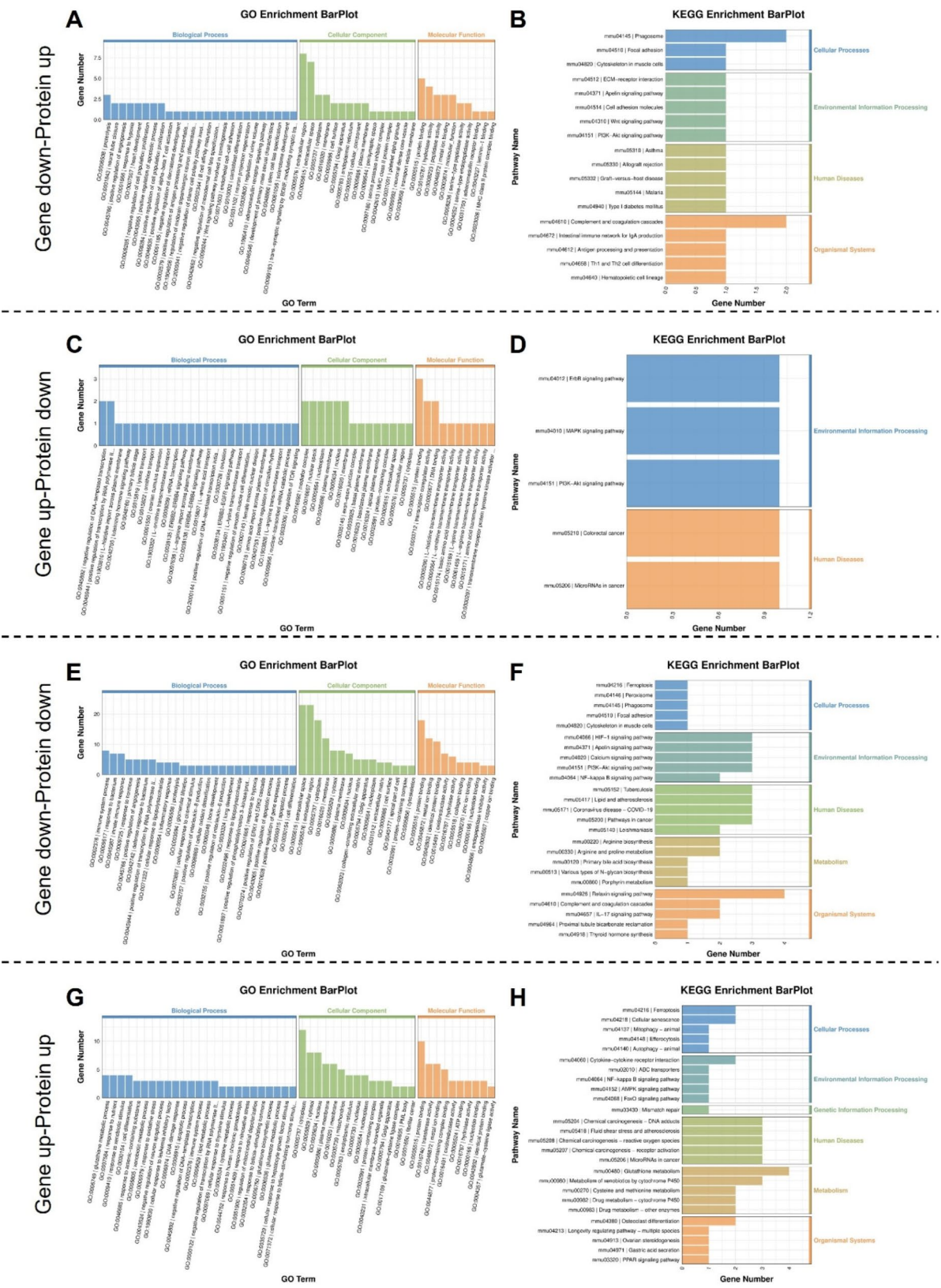


Fig. 6 (See legend on next page.)

(See figure on previous page.)

Fig. 6 Differential GO and KEGG Enrichment Analysis in Gene and Protein Expression Across Que-Exo-Treated Chondrocytes. **(A)** GO enrichment analysis for downregulated genes and upregulated proteins. **(B)** KEGG pathway enrichment analysis. **(C)** GO enrichment analysis for upregulated genes and downregulated proteins. **(D)** KEGG pathway enrichment analysis of upregulated genes and downregulated proteins. **(E)** GO enrichment analysis for downregulated genes and downregulated proteins. **(F)** KEGG pathway enrichment analysis of downregulated genes and downregulated proteins. **(G)** GO enrichment analysis for upregulated genes and upregulated proteins. **(H)** KEGG pathway enrichment analysis of upregulated genes and upregulated proteins

Protective effect of Que-Exo on osteoarthritis in ACLT-Induced mouse model

Histological analysis of the knee joints in the ACLT-induced osteoarthritis (OA) mouse model revealed the effects of different treatments on cartilage degeneration. Figure 7A shows representative Safranin O and Hematoxylin and Eosin (H&E) staining of the knee joint sections. Safranin O staining (which highlights proteoglycan content) demonstrated significant cartilage degradation in the Normal saline and Exo groups, while the Que-Exo group showed preservation of proteoglycan in the cartilage. H&E staining revealed more severe structural damage in the Normal saline and Exo groups compared to the Que-Exo group, which exhibited less tissue damage and better cartilage integrity.

Figure 7B shows the OARSI (Osteoarthritis Research Society International) score, indicating the severity of cartilage damage. The Que-Exo group exhibited a significantly lower OARSI score compared to the Normal saline and Exo groups, indicating a protective effect on cartilage. The Sham group had the lowest OARSI score, confirming that no OA-induced damage occurred in the control group.

Figure 7C quantifies proteoglycan loss as a percentage relative to total cartilage. The Que-Exo group had significantly less proteoglycan loss compared to the Normal saline and Exo groups, indicating that Que-Exo treatment helped maintain cartilage structure and function. The Sham group showed negligible proteoglycan loss.

Discussion

Osteoarthritis (OA) is a degenerative joint disease that is characterized by cartilage degradation, subchondral bone remodeling, and chronic inflammation, with no effective disease-modifying treatments currently available [33, 34]. Traditional treatments primarily focus on symptom relief, but they fail to address the underlying pathophysiology. In this study, we explored the potential of Que-Exo as a novel therapeutic strategy for OA. Our results demonstrate that Que-Exo not only improves the bioavailability of quercetin but also enhances its chondroprotective and anti-inflammatory effects.

One of the major findings from this study is that Que-Exo significantly reduced the expression of pro-inflammatory genes, such as *Mmp9* and *Cox-2*, in IL-1 β -stimulated chondrocytes, as shown by RT-qPCR and Western blot analyses. Que-Exo also significantly

reduced the protein expression of iNOS, TNF- α , MMP-3, and MMP-13, as confirmed by Western blot analysis. These results highlight that Que-Exo not only attenuates inflammation but also prevents cartilage matrix degradation—two core pathological processes in OA progression. These findings align with previous studies demonstrating that MSC-Exos ameliorate OA cellular pathology [35]. Our study further highlights the synergistic efficacy of quercetin delivery via exosomes, which enables more potent modulation of OA-related gene expression profiles compared to exosomes monotherapy. This enhanced therapeutic outcome may be attributed to quercetin's anti-inflammatory and antioxidant properties [36, 37]. The immunofluorescence staining further confirmed these findings by demonstrating a restoration of Collagen II expression in the Que-Exo group, which was significantly downregulated in the IL-1 β -treated groups [38].

The RNA-seq and proteomic analyses revealed that Que-Exo treatment altered a broad range of pathways related to cellular processes such as cell cycle regulation, neurotrophin signaling, and glutathione metabolism, with the PI3K-AKT signaling pathway being significantly enriched in both gene and protein expression profiles. This pathway is crucial for regulating cell survival, proliferation, and metabolism, and its enrichment suggests that Que-Exo might promote chondrocyte survival and regeneration [39, 40]. Moreover, Gene Ontology (GO) enrichment further highlighted significant biological processes related to RNA metabolic processes and stress responses, which may contribute to cartilage repair and protection in OA [41].

In the ACLT-induced OA mouse model, histological analysis revealed that Que-Exo treatment significantly mitigated cartilage degradation and proteoglycan loss, as indicated by Safranin O and H&E staining. The OARSI score and proteoglycan loss quantification further supported the therapeutic potential of Que-Exo, showing its ability to protect cartilage integrity and reduce the severity of OA. The Que-Exo group exhibited less tissue damage compared to the Normal saline and Exo groups, reinforcing the conclusion that Que-Exo exerts a protective effect on joint cartilage.

These findings collectively suggest that Que-Exo may offer a promising approach for OA treatment by combining the regenerative potential of exosomes with the therapeutic benefits of quercetin. The modulation of inflammatory pathways, enhancement of chondrocyte

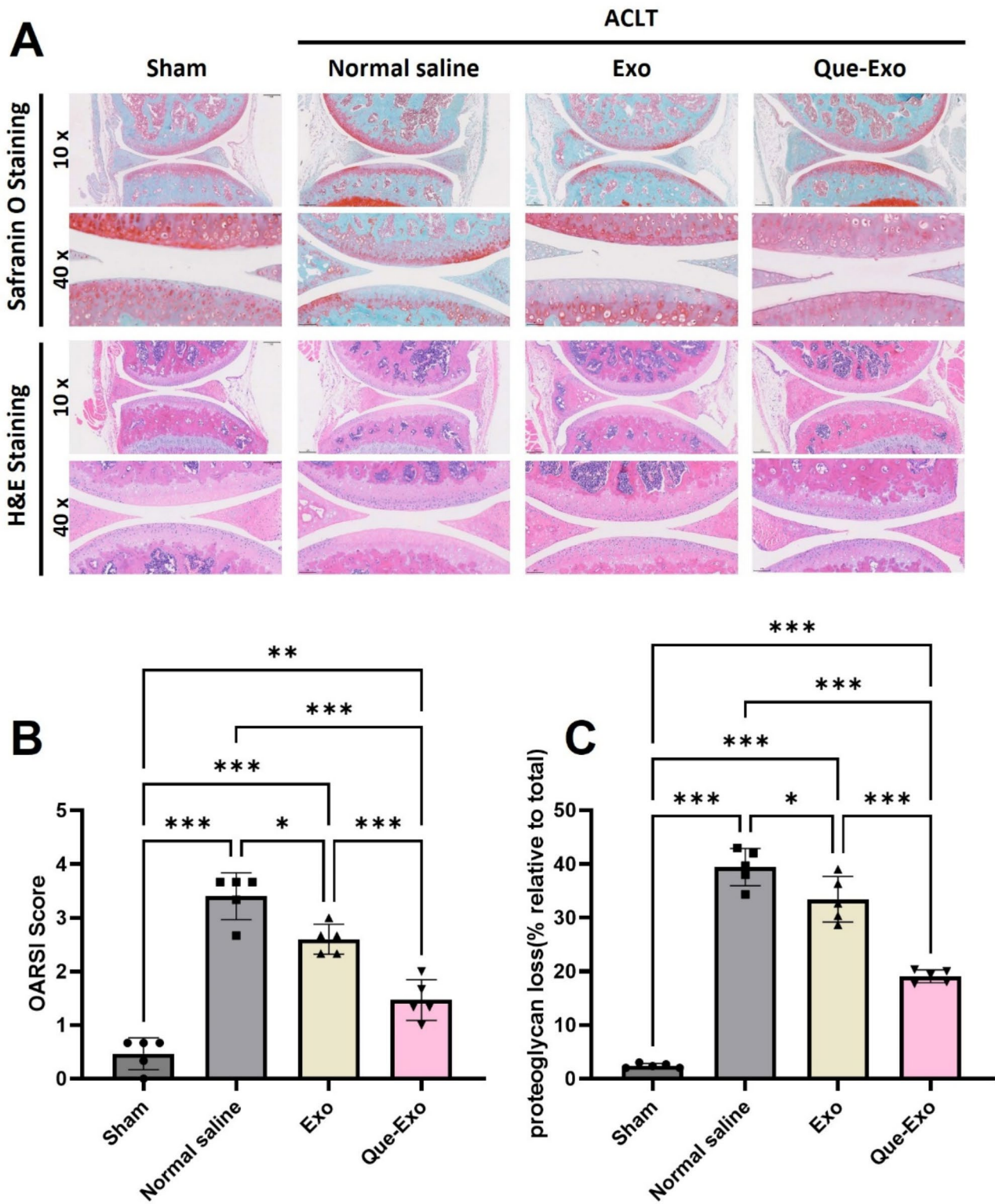


Fig. 7 Protective Effect of Que-Exo on Osteoarthritis in ACLT-Induced Mouse Model. **(A)** Representative Safranin O staining and Hematoxylin and Eosin (H&E) staining of knee joint sections from mice. **(B)** OARSI score. **(C)** Proteoglycan loss as a percentage relative to total cartilage area. The data are presented as mean ± SD. Statistical significance: * $p < 0.05$, ** $p < 0.01$, *** $p < 0.001$

survival, and promotion of cartilage repair observed in this study underscore the translational potential of this novel therapy.

Conclusion

In conclusion, our study demonstrates the potential of Que-Exo as a novel therapeutic strategy for osteoarthritis. By enhancing quercetin's bioavailability and targeting its regenerative effects to chondrocytes, Que-Exo significantly reduces inflammation, promotes cartilage repair, and protects joint integrity in an OA mouse model. The integration of transcriptomic and proteomic data revealed key molecular pathways, particularly the PI3K-AKT signaling pathway, that may mediate these therapeutic effects. Our findings provide a strong foundation for future clinical studies investigating the use of Que-Exo in OA treatment and other degenerative diseases, bridging the gap between traditional herbal medicine and modern regenerative therapies.

Supplementary Information

The online version contains supplementary material available at <https://doi.org/10.1186/s13018-025-05785-1>.

Supplementary Material 1

Acknowledgements

No.

Author contributions

Conceptualization: Mingfeng Lu and Junqing Gao; Methodology: Shilin Li, Lilei He and Aiju Lou; Formal analysis: Mingfeng Lu; Data curation: Mingfeng Lu and Aiju Lou; Validation: Weifeng Fan; Investigation: Weifeng Fan and Lilian Zhao; Funding acquisition: Aiju Lou; Project administration: Lilian Zhao; Writing - original draft preparation: Mingfeng Lu and Aiju Lou; Writing - review and editing: Weifeng Fan and Lilian Zhao; Approval of final manuscript: all authors.

Funding

Guangdong Province Medical Science and Technology Research Foundation Project (A2024661).

Data availability

Data available on request from the authors.

Ethical approval

All experimental procedures involving animals were conducted in strict accordance with the National Institutes of Health Guide for the Care and Use of Laboratory Animals and approved by the Animal Ethics Committee of Guangzhou Shuiyuntian Biotechnology Co., Ltd. (Approval No.: SYT2024087).

Competing interests

The authors declare no competing interests.

Received: 1 March 2025 / Accepted: 3 April 2025

Published online: 15 April 2025

References

- Glyn-Jones S, Palmer AJ, Agricola R, Price AJ, Vincent TL, Weinans H, Carr AJ. Osteoarthritis. *Lancet*. 2015; 386(9991):376–387. [https://doi.org/10.1016/s0140-6736\(14\)60802-3](https://doi.org/10.1016/s0140-6736(14)60802-3)
- Tang S, Zhang C, Oo WM, Fu K, Risberg MA, Bierma-Zeinstra SM, Neogi T, Atukorala I, Malfait AM, Ding C et al. Osteoarthritis. *Nat Rev Dis Primers*. 2025; 11(1):10. <https://doi.org/10.1038/s41572-025-00594-6>
- Wang W, Duan J, Ma W, Xia B, Liu F, Kong Y, Li B, Zhao H, Wang L, Li K, et al. Trimanganese tetroxide nanozyme protects cartilage against degeneration by reducing oxidative stress in osteoarthritis. *Adv Sci (Weinh)*. 2023;10(17):e2205859. <https://doi.org/10.1002/adv.202205859>
- Grässel S, Zaucke F, Madry H. Osteoarthritis: novel molecular mechanisms increase our understanding of the disease pathology. *J Clin Med*. 2021;10(9). <https://doi.org/10.3390/jcm10091938>
- Courties A, Kouki I, Soliman N, Mathieu S, Sellam J. Osteoarthritis year in review 2024: epidemiology and therapy. *Osteoarthritis Cartilage*. 2024;32(11):1397–404. <https://doi.org/10.1016/j.joca.2024.07.014>
- Taruc-Uy RL, Lynch SA. Diagnosis and treatment of osteoarthritis. *Prim Care*. 2013; 40(4):821–836, vii. <https://doi.org/10.1016/j.ppop.2013.08.003>
- Zhou G, Zhang X, Gu Z, Zhao J, Luo M. Research progress in Single-herb Chinese medicine and compound medicine for knee osteoarthritis. *Comb Chem High Throughput Screen*. 2024;27(15):2180–6. <https://doi.org/10.2174/0113862073264850231116055745>
- Wenjin C, Jianwei W. Protective effect of Gentianine, a compound from du Huo Ji Sheng Tang, against Freund's complete Adjuvant-Induced arthritis in rats. *Inflammation*. 2017;40(4):1401–8. <https://doi.org/10.1007/s10753-017-0583-8>
- Chen WJ, Zhuang Y, Peng W, Cui W, Zhang SJ, Wang JW. Du Huo Ji Sheng Tang inhibits Notch1 signaling and subsequent NLRP3 activation to alleviate cartilage degradation in KOA mice. *Chin Med*. 2023;18(1):80. <https://doi.org/10.1186/s13020-023-00784-y>
- Wang JY, Chen WM, Wen CS, Hung SC, Chen PW, Chiu JH. Du-Huo-Ji-Sheng-Tang and its active component ligusticum Chuanxiong promote osteogenic differentiation and decrease the aging process of human mesenchymal stem cells. *J Ethnopharmacol*. 2017;198:64–72. <https://doi.org/10.1016/j.jep.2016.12.011>
- Zhao B, Zhang Q, Liang X, Xie J, Sun Q. Quercetin reduces inflammation in a rat model of diabetic peripheral neuropathy by regulating the TLR4/MyD88/NF- κ B signalling pathway. *Eur J Pharmacol*. 2021;912:174607. <https://doi.org/10.1016/j.ejphar.2021.174607>
- Lu H, Wu L, Liu L, Ruan Q, Zhang X, Hong W, Wu S, Jin G, Bai Y. Quercetin ameliorates kidney injury and fibrosis by modulating M1/M2 macrophage polarization. *Biochem Pharmacol*. 2018;154:203–12. <https://doi.org/10.1016/j.bcp.2018.05.007>
- Li T, Li F, Liu X, Liu J, Li D. Synergistic anti-inflammatory effects of Quercetin and Catechin via inhibiting activation of TLR4-MyD88-mediated NF- κ B and MAPK signaling pathways. *Phytother Res*. 2019;33(3):756–67. <https://doi.org/10.1002/ptr.6268>
- Cui Z, Zhao X, Amevor FK, Du X, Wang Y, Li D, Shu G, Tian Y, Zhao X. Therapeutic application of Quercetin in aging-related diseases: SIRT1 as a potential mechanism. *Front Immunol*. 2022;13:943321. <https://doi.org/10.3389/fimmu.2022.943321>
- Mi Y, Zhong L, Lu S, Hu P, Pan Y, Ma X, Yan B, Wei Z, Yang G. Quercetin promotes cutaneous wound healing in mice through Wnt/ β -catenin signaling pathway. *J Ethnopharmacol*. 2022;290:115066. <https://doi.org/10.1016/j.jep.2022.115066>
- de Vries JH, Hollman PC, Meyboom S, Buysman MN, Zock PL, van Staveren WA, Katan MB. Plasma concentrations and urinary excretion of the antioxidant flavonols Quercetin and Kaempferol as biomarkers for dietary intake. *Am J Clin Nutr*. 1998;68(1):60–5. <https://doi.org/10.1093/ajcn/68.1.60>
- Alizadeh SR, Ebrahimpour MA. Quercetin derivatives: drug design, development, and biological activities, a review. *Eur J Med Chem*. 2022;229:114068. <https://doi.org/10.1016/j.ejmech.2021.114068>
- Lei F, Li M, Lin T, Zhou H, Wang F, Su X. Treatment of inflammatory bone loss in periodontitis by stem cell-derived exosomes. *Acta Biomater*. 2022;141:333–43. <https://doi.org/10.1016/j.actbio.2021.12.035>
- Wen Z, Mai Z, Zhu X, Wu T, Chen Y, Geng D, Wang J. Mesenchymal stem cell-derived exosomes ameliorate cardiomyocyte apoptosis in hypoxic conditions through microRNA144 by targeting the PTEN/AKT pathway. *Stem Cell Res Ther*. 2020;11(1):36. <https://doi.org/10.1186/s13287-020-1563-8>
- Gupta A, Shivaji K, Kadam S, Gupta M, Rodriguez HC, Potty AG, El-Amin SF 3rd, Maffulli N. Immunomodulatory extracellular vesicles: an alternative to cell therapy for COVID-19. *Expert Opin Biol Ther*. 2021;21(12):1551–60. <https://doi.org/10.1080/14712598.2021.1921141>
- Liu S, Fan M, Xu JX, Yang LJ, Qi CC, Xia QR, Ge JF. Exosomes derived from bone-marrow mesenchymal stem cells alleviate cognitive decline in AD-like

- mice by improving BDNF-related neuropathology. *J Neuroinflammation*. 2022;19(1):35. <https://doi.org/10.1186/s12974-022-02393-2>.
22. Gupta A, Cady C, Fauser AM, Rodriguez HC, Mistovich RJ, Potty AGR, Maffulli N. Cell-free stem Cell-Derived extract formulation for regenerative medicine applications. *Int J Mol Sci*. 2020;21(24). <https://doi.org/10.3390/ijms21249364>.
 23. Wan J, He Z, Peng R, Wu X, Zhu Z, Cui J, Hao X, Chen A, Zhang J, Cheng P. Injectable Photocrosslinking spherical hydrogel-encapsulated targeting peptide-modified engineered exosomes for osteoarthritis therapy. *J Nanobiotechnol*. 2023;21(1):284. <https://doi.org/10.1186/s12951-023-02050-7>.
 24. Zhao S, Xiu G, Wang J, Wen Y, Lu J, Wu B, Wang G, Yang D, Ling B, Du D, et al. Engineering exosomes derived from subcutaneous fat MSCs specially promote cartilage repair as miR-199a-3p delivery vehicles in osteoarthritis. *J Nanobiotechnol*. 2023;21(1):341. <https://doi.org/10.1186/s12951-023-02086-9>.
 25. Jin Y, Xu M, Zhu H, Dong C, Ji J, Liu Y, Deng A, Gu Z. Therapeutic effects of bone marrow mesenchymal stem cells-derived exosomes on osteoarthritis. *J Cell Mol Med*. 2021;25(19):9281–94. <https://doi.org/10.1111/jcmm.16860>.
 26. Hu Y, Liu HX, Xu D, Xue X, Xu X. The Anti-Inflammatory effect of miR-140-3p in BMSCs-Exosomes on osteoarthritis. *Acta Chir Orthop Traumatol Cech*. 2023;90(4):267–76.
 27. Xia Q, Wang Q, Lin F, Wang J. miR-125a-5p-abundant exosomes derived from mesenchymal stem cells suppress chondrocyte degeneration via targeting E2F2 in traumatic osteoarthritis. *Bioengineered*. 2021;12(2):11225–38. <https://doi.org/10.1080/21655979.2021.1995580>.
 28. Zhang S, Teo KYW, Chuah SJ, Lai RC, Lim SK, Toh WS. MSC exosomes alleviate temporomandibular joint osteoarthritis by attenuating inflammation and restoring matrix homeostasis. *Biomaterials*. 2019;200:35–47. <https://doi.org/10.1016/j.biomaterials.2019.02.006>.
 29. Cheng S, Xu X, Wang R, Chen W, Qin K, Yan J. Chondroprotective effects of bone marrow mesenchymal stem cell-derived exosomes in osteoarthritis. *J Bioenerg Biomembr*. 2024;56(1):31–44. <https://doi.org/10.1007/s10863-023-09991-6>.
 30. Sun Y, Wang C, Wen L, Ling Z, Xia J, Cheng B, Peng J. Quercetin ameliorates senescence and promotes osteogenesis of BMSCs by suppressing the repetitive element-triggered RNA sensing pathway. *Int J Mol Med*. 2025;55(1). <http://doi.org/10.3892/ijmm.2024.5445>.
 31. Liang H, Yan Y, Sun W, Ma X, Su Z, Liu Z, Chen Y, Yu B. Preparation of Melatonin-Loaded nanoparticles with targeting and sustained release function and their application in osteoarthritis. *Int J Mol Sci*. 2023;24(10). <https://doi.org/10.3390/ijms24108740>.
 32. He L, He T, Xing J, Zhou Q, Fan L, Liu C, Chen Y, Wu D, Tian Z, Liu B, et al. Bone marrow mesenchymal stem cell-derived exosomes protect cartilage damage and relieve knee osteoarthritis pain in a rat model of osteoarthritis. *Stem Cell Res Ther*. 2020;11(1):276. <https://doi.org/10.1186/s13287-020-01781-w>.
 33. Martel-Pelletier J, Barr AJ, Cicuttini FM, Conaghan PG, Cooper C, Goldring MB, Goldring SR, Jones G, Teichtahl AJ, Pelletier JP. Osteoarthritis. *Nat Rev Dis Primers*. 2016;2:16072. <https://doi.org/10.1038/nrdp.2016.72>.
 34. Abramoff B, Caldera FE. Osteoarthritis: pathology, diagnosis, and treatment options. *Med Clin North Am*. 2020;104(2):293–311. <https://doi.org/10.1016/j.mcna.2019.10.007>.
 35. Luo D, Zhu H, Li S, Wang Z, Xiao J. Mesenchymal stem cell-derived exosomes as a promising cell-free therapy for knee osteoarthritis. *Front Bioeng Biotechnol*. 2024;12:1309946. <https://doi.org/10.3389/fbioe.2024.1309946>.
 36. Xu D, Hu MJ, Wang YQ, Cui YL. Antioxidant activities of Quercetin and its complexes for medicinal application. *Molecules*. 2019;24(6). <https://doi.org/10.3390/molecules24061123>.
 37. Shen P, Lin W, Deng X, Ba X, Han L, Chen Z, Qin K, Huang Y, Tu S. Potential implications of Quercetin in autoimmune diseases. *Front Immunol*. 2021;12:689044. <https://doi.org/10.3389/fimmu.2021.689044>.
 38. Xu R, Wu J, Zheng L, Zhao M. Undenatured type II collagen and its role in improving osteoarthritis. *Ageing Res Rev*. 2023;91:102080. <https://doi.org/10.1016/j.arr.2023.102080>.
 39. Sun K, Luo J, Guo J, Yao X, Jing X, Guo F. The PI3K/AKT/mTOR signaling pathway in osteoarthritis: a narrative review. *Osteoarthritis Cartilage*. 2020;28(4):400–9. <https://doi.org/10.1016/j.joca.2020.02.027>.
 40. Xu K, He Y, Moqbel SAA, Zhou X, Wu L, Bao J. SIRT3 ameliorates osteoarthritis via regulating chondrocyte autophagy and apoptosis through the PI3K/Akt/mTOR pathway. *Int J Biol Macromol*. 2021;175:351–60. <https://doi.org/10.1016/j.ijbiomac.2021.02.029>.
 41. Wang S, Li W, Zhang P, Wang Z, Ma X, Liu C, Vasilev K, Zhang L, Zhou X, Liu L, et al. Mechanical overloading induces GPX4-regulated chondrocyte ferroptosis in osteoarthritis via Piezo1 channel facilitated calcium influx. *J Adv Res*. 2022;41:63–75. <https://doi.org/10.1016/j.jare.2022.01.004>.

Publisher's note

Springer Nature remains neutral with regard to jurisdictional claims in published maps and institutional affiliations.